small methods
www.small-methods.com

Unraveling the Degradation Pathway of Inverted Perovskite Solar Cells Based on ISOS-D-1 Protocol

Bowei Li, Jun Deng, K. D. G. Imalka Jayawardena, Xueping Liu, Yuren Xiang, Aobo Ren, Abayomi Titilope Oluwabi, Steven Hinder, Benjamin Putland, John F. Watts, Hui Li, Shixuan Du, S. Ravi P. Silva, and Wei Zhang**

Perovskite solar cells (PSCs) have shown rapid development recently, whereas nonideal stability remains the chief obstacle toward commercialization. Thus, it is of utmost importance to probe the degradation pathway for the entire device. Here, the extrinsic stability of inverted PSCs (IPSCs) is investigated by using standard shelf-life testing based on the International Summit on Organic Photovoltaic Stability protocols (ISOS-D-1). During the long-term assessment of 1700 h, the degraded power conversion efficiency is mainly caused by the fill factor (53% retention) and short-circuit current density (71% retention), while the open-circuit voltage still maintains 97% of the initial values. Further absorbance evolution and density functional theory calculations disclose that the perovskite rear-contact side, in particular for the perovskite/fullerene interface, is the predominant degradation pathway. This study contributes to understanding the aging mechanism and enhancing the durability of IPSCs for future applications.

1. Introduction

Over the past decade, tremendous progress has been achieved in perovskite solar cells (PSCs), yielding power conversion efficiencies (PCEs) of 25.8% and 33.2% for single- and multi-junction cells, respectively.[1] Among all types of PSCs, the device based on the positive-intrinsic-negative (*p-i-n*) configuration is attracting more attention thanks to its negligible hysteresis at different scan rates or light intensities,[2,3] robust performance under operational,[4] damp-heating[5] or thermal-cycling measurements,[6] and excellent compatibility on tandem cells, such as perovskite–perovskite,[7] perovskite–copper indium gallium selenide (CIGS),[8] and perovskite–silicon (Si).[9–12] These advantages confer inverted PSCs (IPSCs) as one of the promising candidates in the solar market.[13] However, long-term stability is the main challenge impeding IPSC for further development. To improve the device stability, various approaches have been reported, such as material or interface engineering[5,14] and encapsulation processing.[15,16] Nonetheless, these strategies have their intrinsic limitations. The engineering methods generally require precise control in the fabrication process, such as the formation of a 2D capping layer[5,17] or the water-insoluble layer through surface reaction.[18,19] Certain interlayer materials can have a contrasting impact on efficiency and stability (e.g., lithium fluoride, LiF[20]). For encapsulation processing, it can increase labor costs[21] and introduce uncertainties during the packaging, including the reaction between encapsulants and perovskite.[22] Furthermore, even after encapsulation, the devices could still contact air via the electrical feedthrough.[23] Due to the presence of variable materials and protocols, encapsulation processing causes difficulty in interlaboratory comparison, leading to an overestimation of the actual lifetime and hindering

B. Li, K. D. G. I. Jayawardena, X. Liu, Y. Xiang, A. T. Oluwabi, H. Li, S. R. P. Silva, W. Zhang
Advanced Technology Institute
Department of Electrical and Electronic Engineering
University of Surrey
GuildfordGU2 7XH, UK
E-mail: s.silva@surrey.ac.uk; wz0003@surrey.ac.uk

J. Deng, H. Li, S. Du
Beijing National Laboratory for Condensed Matter Physics
Institute of Physics
Chinese Academy of Sciences
Beijing100190, China

A. Ren
Institute of Fundamental and Frontier Sciences
University of Electronic Science and Technology of China
Chengdu610054, China

S. Hinder, J. F. Watts
The Surface Analysis Laboratory
Department of Mechanical Engineering Sciences
University of Surrey
Guildford, Surrey GU2 7XH, UK

B. Putland
Clarendon Laboratory
Department of Physics
University of Oxford
OxfordOX1 3PU, UK

The ORCID identification number(s) for the author(s) of this article can be found under https://doi.org/10.1002/smtd.202300223

DOI: 10.1002/smtd.202300223

a comprehensive understanding of the underlying degradation. For example, the significance of extrinsic stability, the device performance under extrinsic factors (e.g., oxygen and/or moisture), is normally undermined or exaggerated within the context of encapsulation.[24] Therefore, in order to accurately assess the extrinsic stability and its related degradation pathway, it is advisable to investigate the tracking performance of the unencapsulated and unmodified devices, like the control or benchmark cells based on the optimized fabrication.

In this study, we conducted the shelf-life (dark storage) stability by using the standard International Summit on Organic Photovoltaic Stability (ISOS-D-1) protocol.[25] All devices were unencapsulated and stored under ambient conditions with continuously monitored temperature (*T*, with an average of 20.2 ± 0. 4 °C) and relative humidity (*RH*, with an average of 40 ± 7%). To evaluate performance stability, the photovoltaic parameters were measured for 1700 h. The long-term shelf-life testing demonstrated that the PCE reduction is dominant by the fill factor (FF) and short-circuit current density (J_{SC}), while the open-circuit voltage (V_{OC}) did not show a noticeable decrease. To make further knowledge of the degradation pathways, we tracked the perovskite film for 1000 h under a humidity of over 66%. Based on the evolution of ultraviolet–visible (UV–vis) absorption spectra, the fullerene material shows a clear "protection effect" that can retard the degradation of the buried perovskite. Further theoretical calculation demonstrated that the perovskite/PCBM interface is the main pathway inducing device aging in the ISOS-D-1 testing.

2. Results and Discussion

2.1. Photovoltaic Performance of IPSCs

The IPSC devices were fabricated using a perovskite light absorber with a strict stoichiometric ratio, without any excess composition (see details in the Experimental Section, Supporting Information). The thickness of as-crystallized perovskite film is around 550 nm, confirmed by a cross-sectional image (Figure S1, Supporting Information) from scanning electron microscopy (SEM) and step measurement from a surface profilometer (Figure S2a, Supporting Information). The optical bandgap (E_g) of the perovskite layer is ≈1.64 eV (Figure S2b, Supporting Information). The poly[N,N′-bis(4-butylphenyl)-N,N′-bis(phenyl)benzidine] (poly-TPD) and [6,6]-phenyl-C61-butyric acid methyl ester (PCBM) layers are serving as the hole transport layer (HTL) and electron transport layer (ETL), respectively (see in **Figure 1**a). To avoid chemical residue and diffusion,[2] UV–ozone treatment is adopted for hydrophobic poly-TPD to enable the full coverage of the perovskite film.[26] Aside from the HTL and ETL, the bathocuproine (BCP) function layer (also called the buffer layer) is introduced to suppress the charge recombination between ETL and metal electrodes.[27,28] All these functional layers are solution-processed at low temperatures, making them well-suited for the upscaling manufacture of minimodules (see Figures S3 and S4, Supporting Information).

To accurately evaluate the device performance, we continuously fabricated 36 devices in three separate batches and measured them outside the glove box. The data of 35 devices were finally obtained (the yield of working devices is 97%) and their corresponding photovoltaic parameters are shown in Figure S5 (Supporting Information). The average V_{OC} is 1.08 ± 0.01 V (arithmetic mean ± standard deviation), FF is 0.77 ± 0.03, and J_{SC} is 21.14 ± 0.32 mA cm^{-2}, all of which contribute to an average PCE of 17.57 ± 0.77%. As shown in Figure 1b–e, the narrow distribution in the overall histograms indicated exceptional reproducibility. The champion performance showed a PCE of 18.80% (with a V_{OC} of 1.09 V, a FF of 0.79, and a J_{SC} of 21.94 mA cm^{-2}). In addition to negligible hysteresis in the current density–voltage (*J–V*) curves (Figure 1f), these PCEs are higher than the previous report based on the same UV-ozone-treated HTL,[26] suggesting an optimized process for our fabrication. The difference between the measured J_{SC} and integrated J_{SC} is within 6%, confirmed by the external quantum efficiency (EQE) spectrum (Figure S6a, Supporting Information). We determined the electronic bandgap of ≈1.64 eV from the EQE plot (Figure S6b, Supporting Information), in good agreement with the above optical bandgap. To verify the PCE value, the operational stability was performed at V_{MPP} (constant voltage at maximum power point, MPP). As shown in Figure 1g, the stabilized PCE exhibits an average value of 18.57%, which is close to the data extracted from the *J–V* curves. After stabilized tracking, two stringent *J–V* characterizations were conducted under various scan rates and light intensities. As seen in Figure 1h,i, the negligible hysteresis is observed either from 25 to 400 mV s^{-1} or from 0.1 to 1 Sun (see details in Figure S7, Supporting Information), indicative of the independent performance[29] and data reliability.

2.2. Shelf-Life Testing of IPSCs

Based on the statistical and operational data, the fabricated devices show reliable photovoltaic parameters and excellent reproducibility, both of which are beneficial for the stability study. Hence, three independent substrates with nine devices (each substrate has three devices) were randomly selected for long-term shelf-life testing. Specifically, all devices were stored in a standard petri dish without any encapsulations in dark under ambient conditions ($T = 20.2 \pm 0.4$ °C and $RH = 40 \pm 7$%, see inset of **Figure 2**a). According to the recent statement for stability assessment,[25] this measurement is classified as ISOS-D-1 protocol, which can reflect the device tolerance to the atmospheric species.

As shown in Figure 2a, the devices were captured at 0, 700, 1300, and 1700 h, respectively. Although the silver (Ag) electrode lost the metallic luster after 1700 h, it remained operational for *J–V* characterization. In Figure 2b–g, a clear "S shape" is observed, with increased series resistance (R_S) and decreased shunt resistance (R_{SH}). More R_S variations indicated the vulnerable FF,[30] which could be caused by degradation of the interfacial contacts.[31] During the ISOS-D-1 testing, unencapsulated devices were periodically measured and the corresponding initial and final performances are listed in Table S1 (Supporting Information). Based on the average data, the PCEs retained 37% of their initial values (17.68 ± 0.67% vs 6.47 ± 0.75%). The reduction is mainly caused by the FF (from 0.78 ± 0.03 to 0.42 ± 0.03) and J_{SC} (from 21.04 ± 0.37 to 14.85 ± 0.96 mA cm^{-2}), while the device V_{OC} remains largely unchanged, with a drop of only 3%. These results indicate that the V_{OC} exhibits higher tolerance to environmental stressors than J_{SC} and FF.

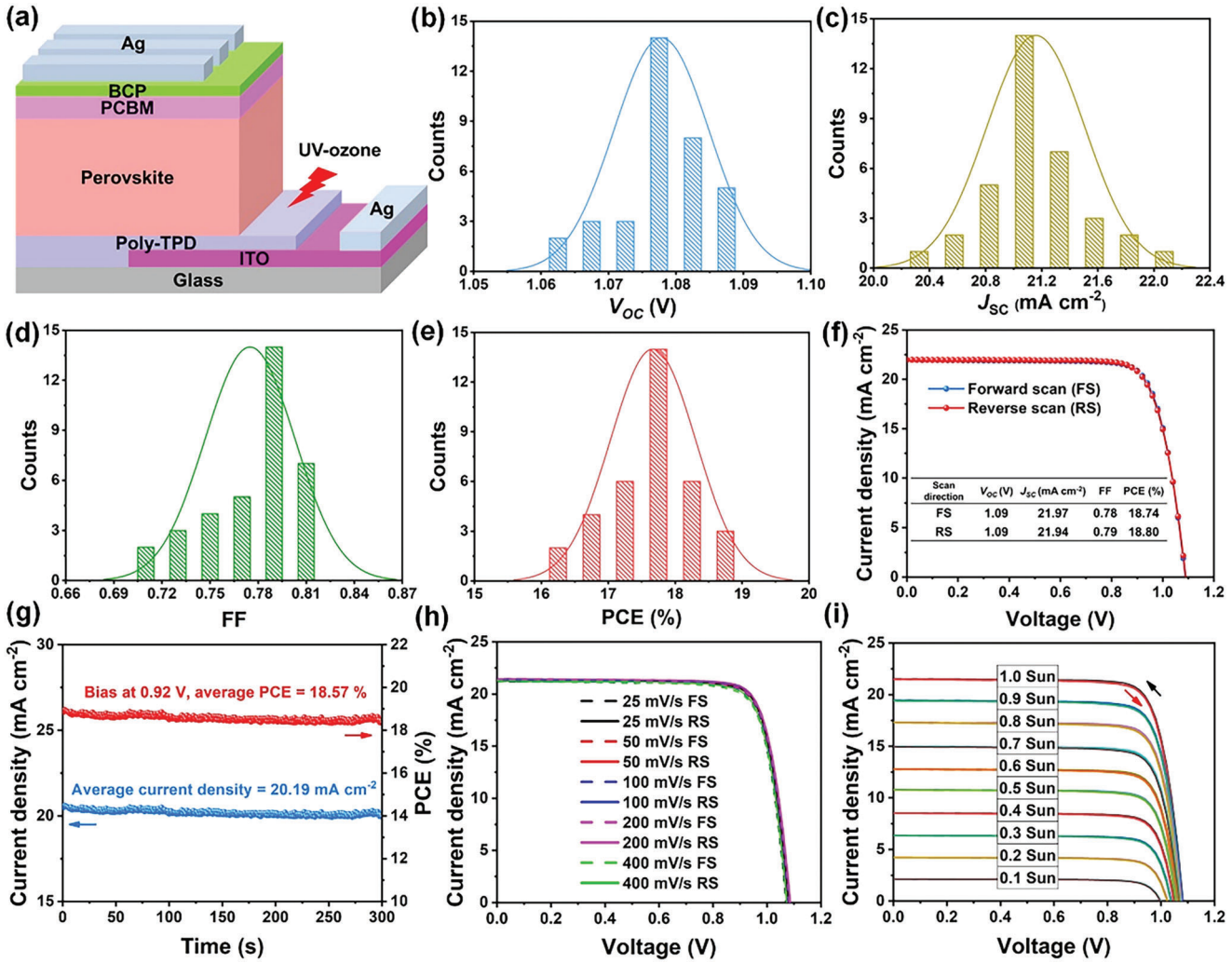

Figure 1. The device structure and performance. a) Schematic configuration. b–e) Histogram of statistical photovoltaic parameters: V_{OC}, J_{SC}, FF, and PCE. For each device, the results shown here are average values from the forward scan (FS, −0.2 to 1.2 V) and reverse scan (RS, 1.2 to −0.2 V). The performance of the champion device, including the f) *J–V* curves and g) stabilized output determined at V_{MPP}. *J–V* curves under different h) scan rates and i) light intensities. Note that the devices were only scanned once and measured outside the glove box without any encapsulation. The temperature (*T*) is 20.9 °C and the relative humidity (*RH*) is 50.1%.

The detailed photovoltaic parameters were recorded as a function of time. In **Figure 3**a–c, the FF and J_{SC} degraded faster than V_{OC}. These different rates imply that the primary sources of instability are stemming from the interfaces,[32] which will be discussed in the following sections. For V_{OC} evolution, the whole process can be divided into three parts: a) from 0 to 600 h, the V_{OC} gradually decreases from 1.08 ± 0.01 to 1.06 ± 0.01 V; b) from 600 to 1200 h, the V_{OC} climbs to a plateau of 1.11 ± 0.01 V. This increase could be attributed to the "self-healing effect" of the perovskite film;[33–35] and c) from 1200 to 1700 h, the V_{OC} reduces to 1.04 ± 0.04 V, which is 97% of the initial values. The small decrease in V_{OC} indicates the perovskite film and poly-TPD are stable as the V_{OC} is strongly determined by the film quality of the light absorber[32,36] and HTL.[37]

In Figure 3d, the device PCEs show a rapid reduction in the initial stage, also known as the "burn-in" region.[38] Through the post-burn-in method (Figure S8, Supporting Information), we extrapolated the data and estimated figures of merit for stability assessment, in which the $T_{Burn\text{-}in}$ (lifetime at the burn-in region) is ≈240 h and the T_{80} (lifetime at 80% of the initial efficiency) is evaluated to be ≈550 h. This "burn-in" effect is related to the ion migration of the A-site cations in perovskite (with a formula of ABX_3)[39] or the interfaces between perovskite and charge transport layers.[32] To further understand the degradation pathway, a systematic analysis of the entire device, including the six functional layers (ITO, poly-TPD, perovskite, PCBM, BCP, Ag), and five interfaces (ITO/poly-TPD, poly-TPD/perovskite, perovskite/PCBM, PCBM/BCP, BCP/Ag), is required.

The bottom ITO substrate and the poly-TPD HTL showed high resistance to moisture ingress[26] and heating stimuli.[14] We intentionally fabricated the poly-TPD-free device and found a dramatically decreased V_{OC} (in Figure S9, Supporting Information). This confirmed the robust poly-TPD layer during the ISOS-D-1 testing, which could be attributed to its

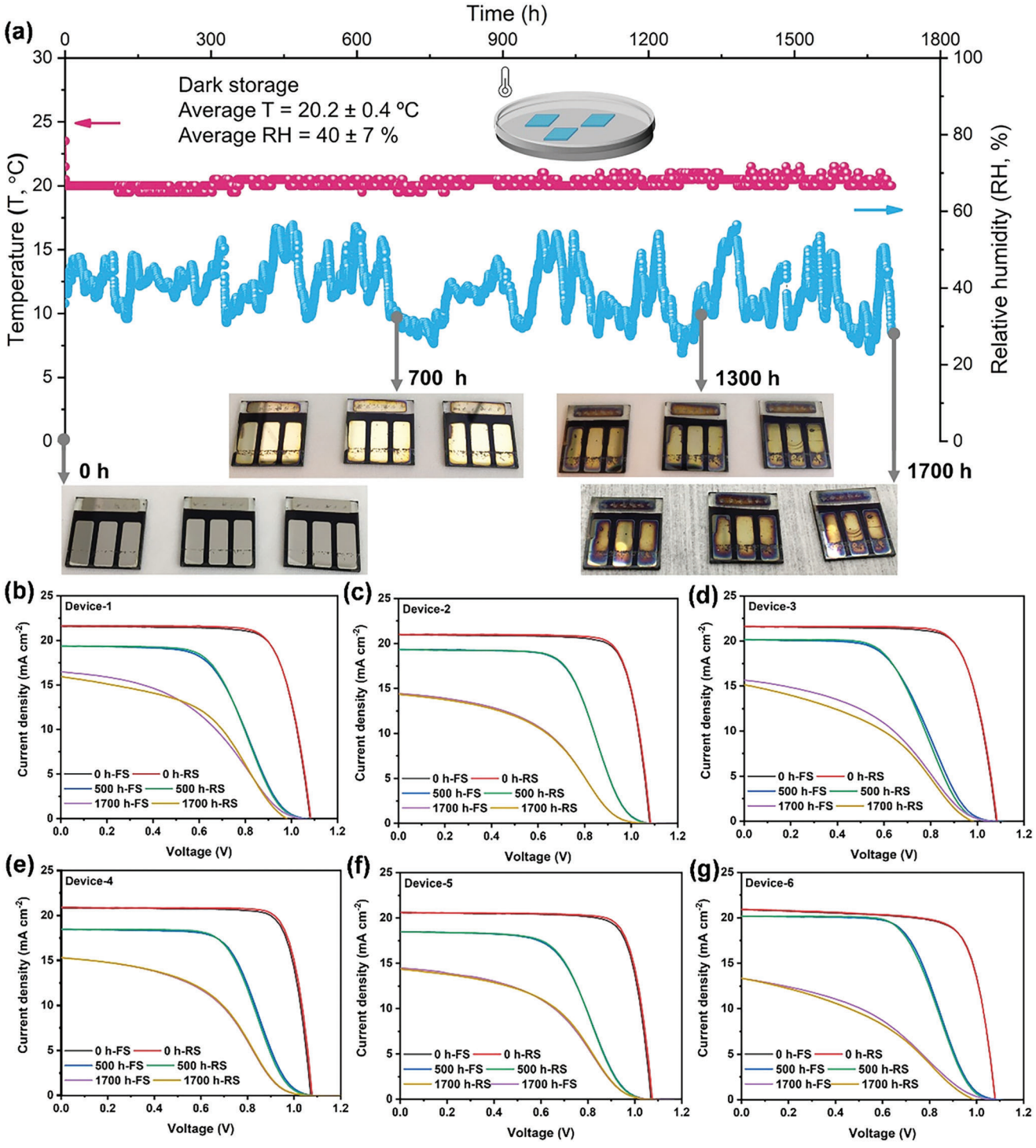

Figure 2. Shelf-life testing based on the ISOS-D-1 protocol. a) Aging process over 1700 h. b–g) The *J–V* curves measured at 0, 500, and 1700 h. The measurements were conducted outside the glove box without any encapsulation. For each *J–V* curve, the devices were only scanned once, consisting of the forward scan (FS, −0.2 to 1.2 V) and reverse scan (RS, 1.2 to −0.2 V). Note that the devices were stored in a petri dish without any encapsulation. The temperature and relative humidity were recorded every 10 min. The inset photographs are the devices captured at the corresponding time. The scratches on the silver electrodes are caused by the clips of the measurement holder.

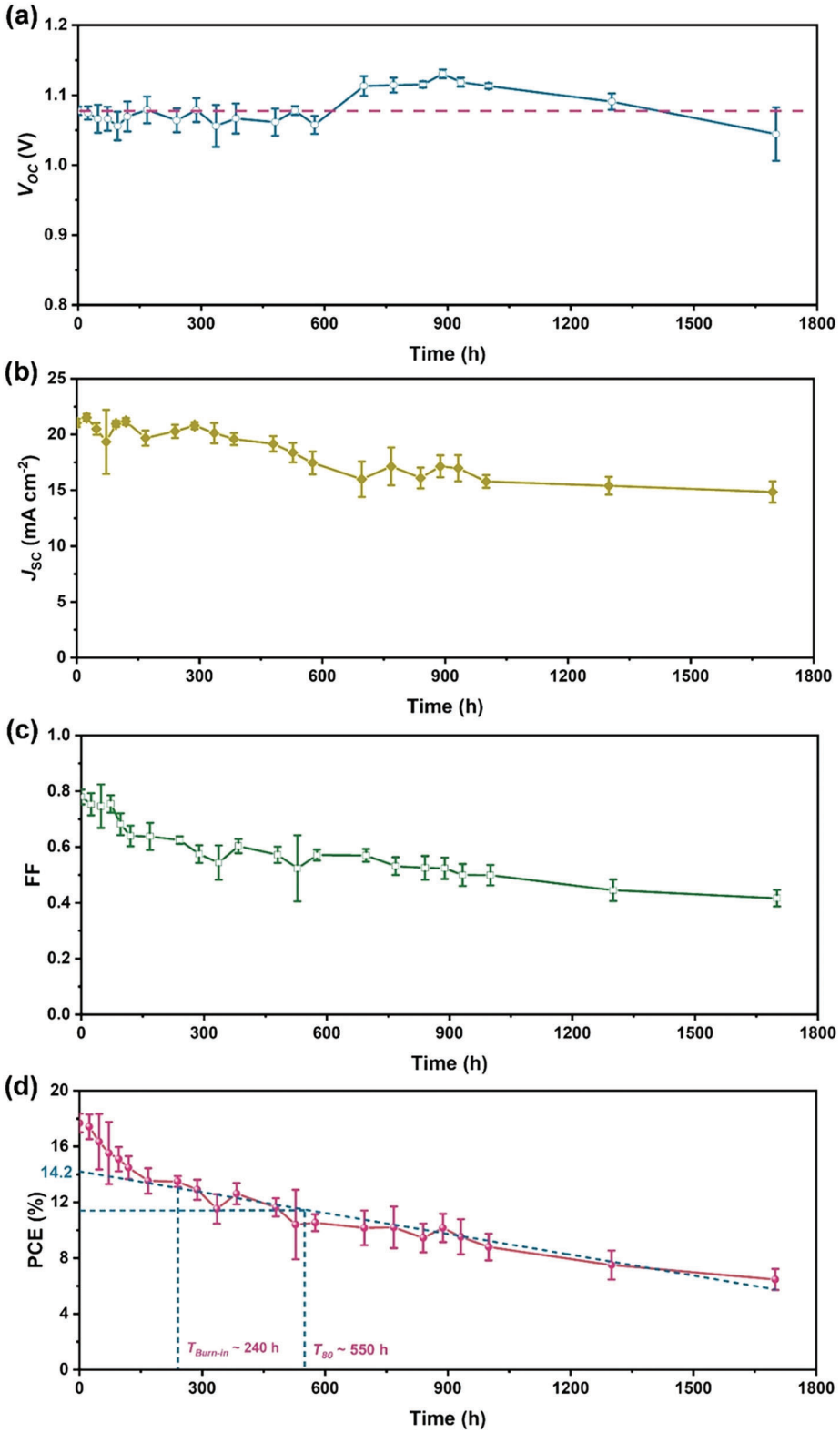

Figure 3. The photovoltaic parameters of devices during the shelf-life testing. a–d) V_{OC}, J_{SC}, FF, and PCE. The data were collected from 6 to 8 devices. For each device, the results shown here are averages from the forward scan (FS, −0.2 to 1.2 V) and reverse scan (RS, 1.2 to −0.2 V). The devices were stored in the dark under lab conditions and measured outside the glove box without any encapsulation. The average T is 20.2 ± 0. 4 °C and RH is 40 ± 7% for 1700 h. $T_{Burn-in}$ indicates the rapid initial degradation time. T_{80} denotes the time of dropping to 80% of the initial efficiency.

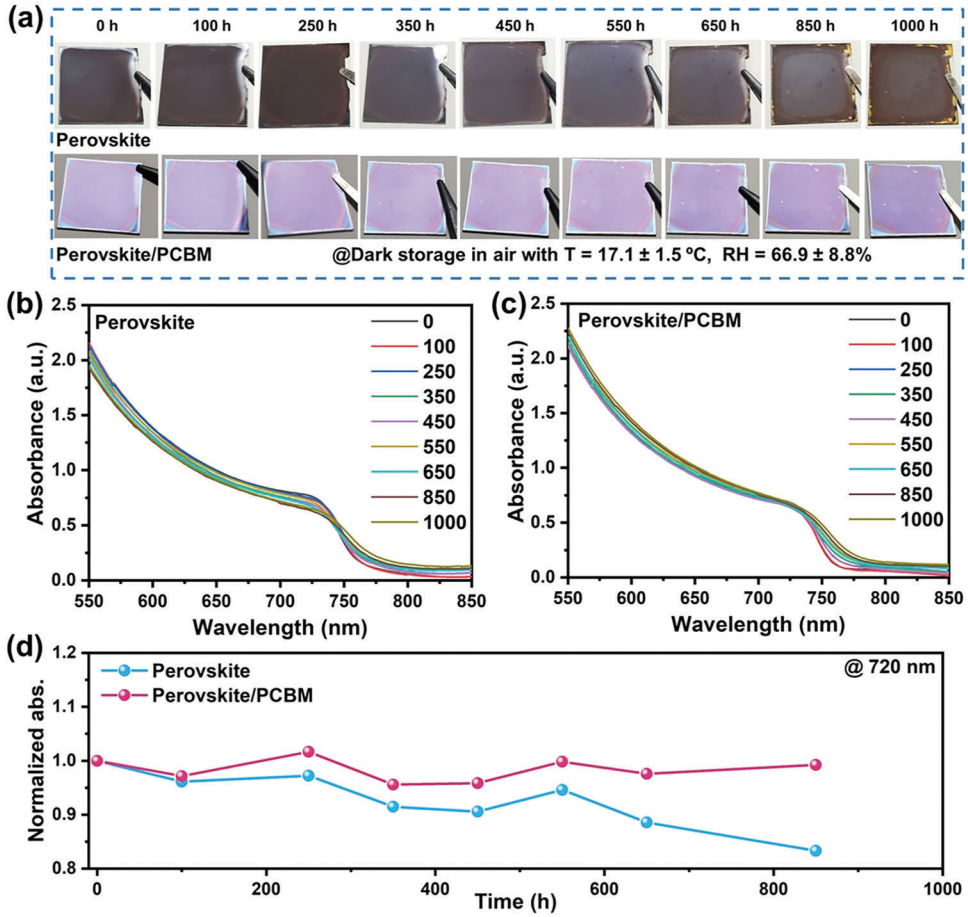

Figure 4. The degradation study of interfaces. a) Photographs of perovskite film with and without PCBM as the function of storage time. The samples were dark stored in a normal petri dish without any encapsulation in ambient conditions. The average *T* is 17.1 ± 1.5 °C and the average *RH* is 66.9 ± 8.8% (see more details in Figure S12, Supporting Information). Evolution of UV–vis light absorption spectra of perovskite film b) without and c) with PCBM. d) Normalized absorbance decay at 720 nm for perovskite films with and without PCBM in ambient conditions without any encapsulation

hydrophobic nature and cross-linking process.[40] Furthermore, our recent study demonstrated low non-radiative losses at the poly-TPD/perovskite interface.[3] Thus, we posit the bottom part is not the major issue in ISOS-D-1 testing. Thanks to contacting charge transport layers, the perovskite is protected by the adjacent functional layers (sandwich structure), without sacrificing the grain size (see SEM images in Figures S10 and S11, Supporting Information) and perovskite phase (see X-ray diffraction [XRD] pattern in Figure S12, Supporting Information). In our study, we adopted the precise stoichiometric perovskite with a formula of $Cs_{0.05}FA_{0.79}MA_{0.16}PbI_{2.4}Br_{0.6}$ (MA denotes $CH_3NH_3^+$, FA denotes $CH(NH_2)_2^+$, Cs denotes cesium, see more details in the Supporting Information). We chose this composition because the triple-cation perovskite (FAMACs) is more stable to surroundings compared to single cation (MA) or binary cations (FAMA).[41]

In light of the above findings, we shift our research focus to the structural properties and performance of the upper parts in devices. For top metal electrodes, the Ag offers excellent electrical conductivity for device measurements (see the *J*–*V* curves in Figure 2), despite tarnishing as a function of the storage time. If the Ag electrode was damaged, the device cannot be measured as normal (see Figure S13, Supporting Information). In addition, the time-of-flight secondary-ion mass spectroscopy (ToF-SIMS) results indicated that Ag cannot diffuse through the PCBM layer into the perovskite during long-term ISOS-D-1 conditions (Figures S14–S16, Table S2, Supporting Information). Hence, these phenomena exclude the Ag electrode as the main degradation pathway for device performance. With the low thickness (≈5 nm), the BCP can be regarded as one of the interfacial strategies between PCBM and Ag thanks to inhibiting charge accumulation.[28] From the chemical structure, the BCP is air-stable at room temperature due to preventing water permeation.[27,42] More importantly, a recent study found that the solution-processed BCP showed better stability than the thermal evaporated.[14,43] Based on these advantages, the BCP layer is not likely to be the main origin of instability in our device. Therefore, we will focus on the PCBM ETL and the perovskite/PCBM interface in the following sections.

2.3. Underlying Degradation Pathway of IPSCs

Aside from acting as ETL, PCBM can passivate the perovskite traps and thus improve the device performance.[44] However, the incomplete coverage or self-degradation of PCBM could cause

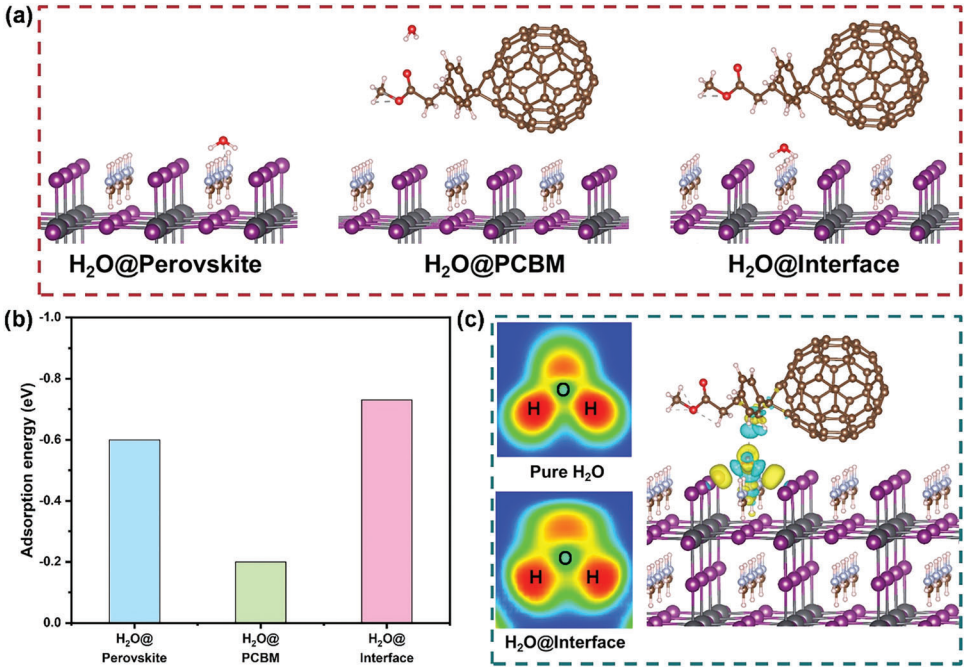

Figure 5. The DFT calculation of interaction between water and perovskite surface without and with PCBM. a) Theoretical models. b) The adsorption energies. c) The electron localization function (ELF) for pure H_2O and H_2O at the interface of PCBM/perovskite and corresponding charge density difference (CDD).

device aging.[45] Here, the PCBM layer is found to fully cover the perovskite film (**Figure 4**a) so the degradation induced by environmental factors could be the origin of instability.[46] We thus tracked the perovskite and perovskite/PCBM film in ambient conditions with a high humidity of 66.9 ± 8.8% (see details in Figure S17, Supporting Information). As shown in Figure 4a, the PCBM did not show the film change after 1000 h, indicative of the stability in ambient conditions. For an extended storage time, the PCBM layer was found to physically protect the buried perovskite film, as compared to the obvious color change from dark to yellow at the edge area for a neat perovskite film (see the photographs in Figures S10 and S11, Supporting Information). The film stability can be further evaluated by analyzing the evolution of the absorbance spectra.[18,47] In Figure 4b,c, both samples showed a redshift in the absorption edge, which could be attributed to either mixing of the halides or environmental stressors.[14] Given that the films are stored in a dark environment (ISOS-D-1), devoid of any heat or bias, we posit that the phase segregation is not a predominant concern. The EQE spectrum of the aged devices exhibited only a minor redshift (Figure S18, Supporting Information). When PCBM was deposited on the surface, the perovskite film did not show an absorbance loss after 850 h (Figure 4d). By contrast, the perovskite film only maintained ≈80% of its initial absorbance. This observation implies that the presence of PCBM can effectively mitigate the impact of environmental stressors on the perovskite film, which is also supported by the steady-state photoluminescence (PL) spectra (Figure S19, Supporting Information). The "protection effect" can be ascribed to the multiple functions of the PCBM layer, consisting of passivating the trap states, preventing electrode damage and resisting moisture.[44,48]

The above results suggested that the PCBM layer is not the main degradation pathway. We thus focus on the perovskite/PCBM interface, which plays an important role as the interfacial losses could impair the device performance.[3,49] Due to the readily volatilized organic cations or halides in the annealing process, the perovskite surface or grain boundaries inevitably exist many defects, such as the undercoordinated leads or halides, lead clusters, and organic or halide vacancies.[50] In addition, these defects are electrically charged, which can accelerate the device aging under environmental stressors. In the ISOS-D-1 testing, the environmental stressors involve temperature, oxygen, and moisture. Given that the temperature is similar to the room temperature (Figure S17, Supporting Information) and that exposure to pure oxygen has shown minimal damage or weak interaction to the perovskite[21] or PCBM[46,51] at dark storage, we highlight moisture as the potential cause of instability. The degradation pathway can be discerned through the examination of the interaction between water and perovskite, PCBM, or their interface.

To probe the possible interactions, we conducted density functional theory (DFT) calculations based on a cubic formamidinium lead halide ($FAPbI_3$) model.[52] As illustrated in **Figure 5**a, one water molecule (H_2O) was introduced on the perovskite surface with and without PCBM treatment. The considered geometrical structures can be found in Figure S20 (Supporting Information). As shown in Figure 5b, the adsorption energy (ΔE_{ads}) is −0.6 eV (water on perovskite surface), −0.2 eV (water on PCBM surface with perovskite at the bottom), and −0.7 eV (water lies at the interface between PCBM and perovskite), separately (Table S3, Supporting Information). By comparing their adsorption energy (−0.6 eV vs −0.2 eV), the water is more readily adsorbed on the perovskite surface than on the PCBM

layer. This observation suggests that the presence of PCBM can effectively inhibit water damage to the buried perovskite film, consistent with the previous discussion. However, the water can deteriorate the perovskite film through the perovskite/PCBM interface. This adsorption process is even faster than the pure perovskite film due to the lower ΔE_{ads} (−0.6 eV vs −0.7 eV). Compared to pure water, the water at the interface has a particular characteristic, in which the lone pair electrons of O and the electrons of H are more easily polarized. This is evidenced by the electron localization function (ELF) and charge density difference (CDD) as illustrated in Figure 5c. The O atoms could form hydrogen bonds with FA^+ ($(NH_2)_2CH^+$) and H atoms would form a hydrogen bond with I^-. In addition, there is a weak interaction between water and PCBM (existing charge transfer in CDD, Figure S21, Supporting Information). These characteristics enable facile water adsorption at the interface. Given the theoretical and experimental results, we demonstrated that the PCBM/perovskite interface is an important pathway during the ISOS-D-1 testing. The adsorbed water could decompose the perovskite film to form halide ions, which can diffuse through the ETL or ETL/Ag interface to react with the Ag (also see Figure S15, Supporting Information).[53–56] Compared to the buried interface (perovskite/poly-TPD), the ion migration tends to occur at the upper interface. As shown in Figures S22–S24 (Supporting Information), cross-sectional SEM images of the aged devices exhibited voids near the perovskite/PCBM interface, confirming the main degradation pathway under environmental stressors.

3. Conclusion

In summary, the extrinsic stability of IPSCs was systematically investigated. Our findings demonstrated that the perovskite/PCBM interface is the main degradation pathway, which is more vulnerable to the moisture stressor and thus induces more interfacial losses for the entire device during the long-term ISOS-D-1 testing. This degradation pathway causes a pronounced impact on the FF and J_{SC}, while only mildly influencing the V_{OC}. Therefore, it is crucially important to strategically optimize the perovskite/PCBM interface in order to achieve stability in devices. Our study offers valuable insights into the advancement of high-performance IPSCs.

4. Experimental Section

Experimental details are provided in the Supporting Information.

Supporting Information

Supporting Information is available from the Wiley Online Library or from the author.

Acknowledgements

W.Z. thanks EPSRC standard research (EP/V027131/1) and Newton Advanced Fellowship (192097) for financial support. B.L. thanks China Scholarship Council (CSC, No. 201706020158) for financial support during his Ph.D. career. K.D.G.I.J. and S.R.P.S. thank European Commission H2020 CORNET program (Grant ID: 760949) and Equal Opportunities Foundation Hong Kong for financial support. H.L. thanks National Key Research and Development Program of China (2019YFB1503500), the State Key Laboratory of Metastable Materials Science and Technology (201901), and Fujian Key Laboratory of Photoelectric Functional Materials (FJPFM-201902) for financial support. A.R. thanks Innovation Group Project of Sichuan Province (20CXTD0090) for financial support.

Conflict of Interest

The authors declare no conflict of interest.

Author Contributions

B.L. conceived the work, fabricated and characterized solar cells. B.L., X.L., and B.P. conducted SEM measurements. J.D. and S.D. conducted the DFT calculations. A.T.O. conducted the laser scribing. S.H. conducted ToF-SIMS. B.L. wrote the draft of the paper, and the other authors contributed to data interpretation or revision of the manuscript. W.Z. and S.R.P. directed and supervised the project.

Data Availability Statement

The data that support the findings of this study are available from the corresponding author upon reasonable request.

Keywords

degradation pathways, inverted perovskite solar cells, ISOS-D-1 testing

Received: February 21, 2023
Revised: May 31, 2023
Published online:

[1] NREL, "Best Research-Cell Efficiencies," https://www.nrel.gov/pv/assets/pdfs/best-research-cell-efficiencies.pdf (accessed: May **2023**).
[2] B. Li, Y. Xiang, K. D. G. I. Jayawardena, D. Luo, Z. Wang, X. Yang, J. F. Watts, S. Hinder, M. T. Sajjad, T. Webb, H. Luo, I. Marko, H. Li, S. A. J. Thomson, R. Zhu, G. Shao, S. J. Sweeney, S. R. P. Silva, W. Zhang, *Nano Energy* **2020**, *78*, 105249.
[3] B. Li, J. Deng, J. A. Smith, P. Caprioglio, K. Ji, D. Luo, J. D. McGettrick, K. D. G. I. Jayawardena, R. C. Kilbride, A. Ren, S. Hinder, J. Bi, T. Webb, I. Marko, X. Liu, Y. Xiang, J. Reding, H. Li, S. Du, D. G. Lidzey, S. D. Stranks, T. Watson, S. Sweeney, H. J. Snaith, S. R. P. Silva, W. Zhang, *Adv. Energy Mater.* **2022**, *12*, 2202868.
[4] Z. Li, B. Li, X. Wu, S. A. Sheppard, S. Zhang, D. Gao, N. J. Long, Z. Zhu, *Science* **2022**, *376*, 416.
[5] R. Azmi, E. Ugur, A. Seitkhan, F. Aljamaan, A. S. Subbiah, J. Liu, G. T. Harrison, M. I. Nugraha, M. K. Eswaran, M. Babics, Y. Chen, F. Xu, T. G. Allen, A. U. Rehman, C. Wang, T. D. Anthopoulos, U. Schwingenschlögl, M. D. Bastiani, E. Aydin, S. D. Wolf, *Science* **2022**, *376*, 73.
[6] G. Li, Z. Su, L. Canil, D. Hughes, M. H. Aldamasy, J. Dagar, S. Trofimov, L. Wang, W. Zuo, J. J. Jerónimo-Rendon, M. M. Byranvand, C. Wang, R. Zhu, Z. Zhang, F. Yang, G. Nasti, B. Naydenov, W. C. Tsoi, Z. Li, X. Gao, Z. Wang, Y. Jia, E. Unger, M. Saliba, M. Li, A. Abate, *Science* **2023**, *379*, 399.
[7] D. P. McMeekin, S. Mahesh, N. K. Noel, M. T. Klug, J. Lim, J. H. Warby, J. M. Ball, L. M. Herz, M. B. Johnston, H. J. Snaith, *Joule* **2019**, *3*, 387.

[8] F. Lang, M. Jošt, K. Frohna, E. Köhnen, A. Al-Ashouri, A. R. Bowman, T. Bertram, A. B. Morales-Vilches, D. Koushik, E. M. Tennyson, K. Galkowski, G. Landi, M. Creatore, B. Stannowski, C. A. Kaufmann, J. Bundesmann, J. Rappich, B. Rech, A. Denker, S. Albrecht, H. C. Neitzert, N. H. Nickel, S. D. Stranks, *Joule* **2020**, *4*, 1054.
[9] L. Mazzarella, Y. H. Lin, S. Kirner, A. B. Morales-Vilches, L. Korte, S. Albrecht, E. Crossland, B. Stannowski, C. Case, H. J. Snaith, R. Schlatmann, *Adv. Energy Mater.* **2019**, *9*, 1803241.
[10] Y. Hou, E. Aydin, M. De Bastiani, C. Xiao, F. H. Isikgor, D. J. Xue, B. Chen, H. Chen, B. Bahrami, A. H. Chowdhury, A. Johnston, S.-W. Baek, Z. Huang, M. Wei, Y. Dong, J. Troughton, R. Jalmood, A. J. Mirabelli, T. G. Allen, E. Van Kerschaver, M. I. Saidaminov, D. Baran, Q. Qiao, K. Zhu, S. De Wolf, E. H. Sargent, *Science* **2020**, *367*, 1135.
[11] J. Xu, C. C. Boyd, Z. J. Yu, A. F. Palmstrom, D. J. Witter, B. W. Larson, R. M. France, J. Werner, S. P. Harvey, E. J. Wolf, W. Weigand, S. Manzoor, M. F. A. M. van Hest, J. J. Berry, J. M. Luther, Z. C. Holman, M. D. McGehee, *Science* **2020**, *367*, 1097.
[12] D. Kim, H. J. Jung, I. J. Park, B. W. Larson, S. P. Dunfield, C. Xiao, J. Kim, J. Tong, P. Boonmongkolras, S. G. Ji, F. Zhang, S. R. Pae, M. Kim, S. B. Kang, V. Dravid, J. J. Berry, J. Y. Kim, K. Zhu, D. H. Kim, B. Shin, *Science* **2020**, *368*, 155.
[13] B. Li, W. Zhang, *Commun. Mater.* **2022**, *3*, 65.
[14] Y. H. Lin, N. Sakai, P. Da, J. Wu, H. C. Sansom, A. J. Ramadan, S. Mahesh, J. Liu, R. D. J. Oliver, J. Lim, L. Aspitarte, K. Sharma, P. K. Madhu, A. B. Morales-Vilches, P. K. Nayak, S. Bai, F. Gao, C. R. M. Grovenor, M. B. Johnston, J. G. Labram, J. R. Durrant, J. M. Ball, B. Wenger, B. Stannowski, H. J. Snaith, *Science* **2020**, *369*, 96.
[15] X. Li, F. Zhang, H. He, J. J. Berry, K. Zhu, T. Xu, *Nature* **2020**, *578*, 555.
[16] L. Shi, M. P. Bucknall, T. L. Young, M. Zhang, L. Hu, J. Bing, D. S. Lee, J. Kim, T. Wu, N. Takamure, D. R. McKenzie, S. Huang, M. A. Green, A. W. Y. Ho-Baillie, *Science* **2020**, *368*, 1309.
[17] H. Chen, S. Teale, B. Chen, Y. Hou, L. Grater, T. Zhu, K. Bertens, S. M. Park, H. R. Atapattu, Y. Gao, M. Wei, A. K. Johnston, Q. Zhou, K. Xu, D. Yu, C. Han, T. Cui, E. H. Jung, C. Zhou, W. Zhou, A. H. Proppe, S. Hoogland, F. Laquai, T. Filleter, K. R. Graham, Z. Ning, E. H. Sargent, *Nat. Photonics* **2022**, *16*, 352.
[18] S. Yang, S. Chen, E. Mosconi, Y. Fang, X. Xiao, C. Wang, Y. Zhou, Z. Yu, J. Zhao, Y. Gao, F. De Angelis, J. Huang, *Science* **2019**, *365*, 473.
[19] X. Li, W. Zhang, X. Guo, C. Lu, J. Wei, J. Fang, *Science* **2022**, *375*, 434.
[20] A. Al-Ashouri, E. Köhnen, B. Li, A. Magomedov, H. Hempel, P. Caprioglio, J. A. Márquez, A. B. Morales Vilches, E. Kasparavicius, J. A. Smith, N. Phung, D. Menzel, M. Grischek, L. Kegelmann, D. Skroblin, C. Gollwitzer, T. Malinauskas, M. Jošt, G. Matič, B. Rech, R. Schlatmann, M. Topič, L. Korte, A. Abate, B. Stannowski, D. Neher, M. Stolterfoht, T. Unold, V. Getautis, S. Albrecht, *Science* **2020**, *370*, 1300.
[21] C. C. Boyd, R. Cheacharoen, T. Leijtens, M. D. McGehee, *Chem. Rev.* **2018**, *119*, 3418.
[22] E. Ramasamy, V. Karthikeyan, K. Rameshkumar, G. Veerappan, *Mater. Lett.* **2019**, *250*, 51.
[23] L. Shi, T. L. Young, J. Kim, Y. Sheng, L. Wang, Y. Chen, Z. Feng, M. J. Keevers, X. Hao, P. J. Verlinden, M. A. Green, A. W. Y. Ho-Baillie, *ACS Appl. Mater. Interfaces* **2017**, *9*, 25073.
[24] S. Ma, G. Yuan, Y. Zhang, N. Yang, Y. Li, Q. Chen, *Energy Environ. Sci.* **2022**, *15*, 13.
[25] M. V. Khenkin, E. A. Katz, A. Abate, G. Bardizza, J. J. Berry, C. Brabec, F. Brunetti, V. Bulović, Q. Burlingame, A. Di Carlo, R. Cheacharoen, Y.-B. Cheng, A. Colsmann, S. Cros, K. Domanski, M. Dusza, C. J. Fell, S. R. Forrest, Y. Galagan, D. Di Girolamo, M. Grätzel, A. Hagfeldt, E. von Hauff, H. Hoppe, J. Kettle, H. Köbler, M. S. Leite, S. (Frank) Liu, Y. L. Loo, J. M. Luther, *Nat. Energy* **2020**, *5*, 35.
[26] X. Xu, C. Ma, Y. Cheng, Y. M. Xie, X. Yi, B. Gautam, S. Chen, H. W. Li, C. S. Lee, F. So, S. W. Tsang, *J. Power Sources* **2017**, *360*, 157.
[27] C. Chen, S. Zhang, S. Wu, W. Zhang, H. Zhu, Z. Xiong, Y. Zhang, W. Chen, *RSC Adv.* **2017**, *7*, 35819.
[28] N. Shibayama, H. Kanda, T. W. Kim, H. Segawa, S. Ito, *APL Mater.* **2019**, *7*, 031117.
[29] Q. Jiang, L. Zhang, H. Wang, X. Yang, J. Meng, H. Liu, Z. Yin, J. Wu, X. Zhang, J. You, *Nat. Energy* **2017**, *2*, 16177.
[30] N. Mundhaas, Z. J. Yu, K. A. Bush, H. P. Wang, J. Häusele, S. Kavadiya, M. D. McGehee, Z. C. Holman, *Sol. RRL* **2019**, *3*, 1800378.
[31] A. Guerrero, J. You, C. Aranda, Y. S. Kang, G. Garcia-Belmonte, H. Zhou, J. Bisquert, Y. Yang, *ACS Nano* **2016**, *10*, 218.
[32] J. A. Christians, P. Schulz, J. S. Tinkham, T. H. Schloemer, S. P. Harvey, B. J. Tremolet de Villers, A. Sellinger, J. J. Berry, J. M. Luther, *Nat. Energy* **2018**, *3*, 68.
[33] Y. Deng, Q. Dong, C. Bi, Y. Yuan, J. Huang, *Adv. Energy Mater.* **2016**, *6*, 1600372.
[34] J. S. Yun, J. Kim, T. Young, R. J. Patterson, D. Kim, J. Seidel, S. Lim, M. A. Green, S. Huang, A. Ho-Baillie, *Adv. Funct. Mater.* **2018**, *28*, 1705363.
[35] G. E. Eperon, S. N. Habisreutinger, T. Leijtens, B. J. Bruijnaers, J. J. Van Franeker, D. W. Dequilettes, S. Pathak, R. J. Sutton, G. Grancini, D. S. Ginger, R. A. J. Janssen, A. Petrozza, H. J. Snaith, *ACS Nano* **2015**, *9*, 9380.
[36] Q. Jiang, Y. Zhao, X. Zhang, X. Yang, Y. Chen, Z. Chu, Q. Ye, X. Li, Z. Yin, J. You, *Nat. Photonics* **2019**, *13*, 460.
[37] Q. Wang, C. Bi, J. Huang, *Nano Energy* **2015**, *15*, 275.
[38] S. Bai, P. Da, C. Li, Z. Wang, Z. Yuan, F. Fu, M. Kawecki, X. Liu, N. Sakai, J. T.-W. Wang, S. Huettner, S. Buecheler, M. Fahlman, F. Gao, H. J. Snaith, *Nature* **2019**, *571*, 245.
[39] K. Domanski, B. Roose, T. Matsui, M. Saliba, S.-H. Turren-Cruz, J. P. Correa-Baena, C. R. Carmona, G. Richardson, J. M. Foster, F. De Angelis, J. M. Ball, A. Petrozza, N. Mine, M. K. Nazeeruddin, W. Tress, M. Grätzel, U. Steiner, A. Hagfeldt, A. Abate, *Energy Environ. Sci.* **2017**, *10*, 604.
[40] B. Li, Y. Xiang, K. D. G. I. Jayawardena, D. Luo, J. F. Watts, S. Hinder, H. Li, V. Ferguson, H. Luo, R. Zhu, S. R. P. Silva, W. Zhang, *Sol. RRL* **2020**, *4*, 2000060.
[41] M. Saliba, T. Matsui, J. Y. Seo, K. Domanski, J. P. Correa-Baena, M. K. Nazeeruddin, S. M. Zakeeruddin, W. Tress, A. Abate, A. Hagfeldt, M. Grätzel, *Energy Environ. Sci.* **2016**, *9*, 1989.
[42] X. Sun, M. Gobbi, A. Bedoya-Pinto, O. Txoperena, F. Golmar, R. Llopis, A. Chuvilin, F. Casanova, L. E. Hueso, *Nat. Commun.* **2013**, *4*, 2794.
[43] Y. Deng, S. Xu, S. Chen, X. Xiao, J. Zhao, J. Huang, *Nat. Energy* **2021**, *6*, 633.
[44] Y. Shao, Z. Xiao, C. Bi, Y. Yuan, J. Huang, *Nat. Commun.* **2014**, *5*, 5784.
[45] J. You, L. Meng, T. Bin Song, T. F. Guo, W. H. Chang, Z. Hong, H. Chen, H. Zhou, Q. Chen, Y. Liu, N. De Marco, Y. Yang, *Nat. Nanotechnol.* **2016**, *11*, 75.
[46] Q. Bao, X. Liu, S. Braun, M. Fahlman, *Adv. Energy Mater.* **2014**, *4*, 1301272.
[47] J. Yang, B. D. Siempelkamp, D. Liu, T. L. Kelly, *ACS Nano* **2015**, *9*, 1955.
[48] Y. Fang, C. Bi, D. Wang, J. Huang, *ACS Energy Lett.* **2017**, *2*, 782.
[49] X. Zheng, B. Chen, J. Dai, Y. Fang, Y. Bai, Y. Lin, H. Wei, X. C. Zeng, J. Huang, *Nat. Energy* **2017**, *2*, 17102.
[50] B. Chen, P. N. Rudd, S. Yang, Y. Yuan, J. Huang, *Chem. Soc. Rev.* **2019**, *48*, 3842.
[51] S. Chambon, A. Rivaton, J. L. Gardette, M. Firon, *Sol. Energy Mater. Sol. Cells* **2007**, *91*, 394.
[52] F. Wang, W. Geng, Y. Zhou, H. Fang, C. Tong, M. A. Loi, L. Liu, N. Zhao, **2016**, 28, 9986.
[53] Y. Kato, L. K. Ono, M. V. Lee, S. Wang, S. R. Raga, Y. Qi, *Adv. Mater. Interfaces* **2015**, *2*, 1500195.
[54] J. Li, Q. Dong, N. Li, L. Wang, *Adv. Energy Mater.* **2017**, *7*, 1602922.
[55] E. J. Juarez-Perez, Z. Hawash, S. R. Raga, L. K. Ono, Y. Qi, *Energy Environ. Sci.* **2016**, *9*, 3406.
[56] D. B. Khadka, Y. Shirai, M. Yanagida, K. Miyano, *ACS Appl. Energy Mater.* **2021**, *4*, 11121.

